International Journal of Heat and Mass Transfer 157 (2020) 119962

Contents lists available at ScienceDirect

International Journal of Heat and Mass Transfer

journal homepage: www.elsevier.com/locate/hmt

A general scaling for the barrier factor of composites containing thin layered flakes of rectangular, circular and hexagonal shape

A. Tsiantis, T.D. Papathanasiou*

Department of Mechanical Engineering, University of Thessaly, Volos, Greece

ARTICLE INFO

Article history:
Received 4 March 2020
Revised 30 April 2020
Accepted 13 May 2020

Keywords:
Diffusion
Materials Modeling
3D Simulation
Barrier properties
Composites
Flakes

ABSTRACT

We propose a general scaling which allows for the results of 3D mass transfer computations in layered flake composites containing square, circular or hexagonal flakes to collapse on a single master curve. We show that the Barrier Improvement Factor ($BIF \sim 1/D_{eff}$) of such composites is well represented by a power function of that scale (M) namely $BIF = (1+M)^2$. Our simulations are carried out in three-dimensional multi-particle RVEs each containing up to 4000 randomly placed individual flakes. The flakes are represented as two-dimensional squares, disks or hexagons; this representation is suitable for very thin flakes, such as exfoliated nano-platelets. Around 3000 simulations are carried out, and the effective BIF is computed for different values of flake orientation, shape, dimensions and number density. We show that our scaling is consistent with the traditional representation of the BIF as a power function of $(\alpha\phi)$, (α) and (ϕ) being the aspect ratio and the volume fraction of the flakes, while at the same time offering a generalized approach that is valid for all flake shapes. When the flakes are layered at an angle (θ) to the direction of macroscopic diffusion, we propose a model for the BIF in terms of the principal diffusivity and (θ); this is found to be in very good agreement with computational results, which show that while the BIF increases with increasing (M), this increase is no longer monotonic but, instead, BIF approaches an asymptotic plateau value which is determined by (θ).

1. Introduction

Flake-filled composites are of interest in applications in which the transport of a species is to be hindered without resorting to the use of expensive and possibly environmentally hazardous additives [1–3]. Notable examples of such "passive" barrier materials can be found in packaging applications [4,5], sound insulation [6], anti-corrosion coatings [7] as well as in fire-retarding polymers [8]. In all cases, the impetus for the use of (essentially) two-dimensional flakes lies in the tortuous internal structure of the corresponding composites, which allows for a substantial improvement ($\sim (\alpha\phi)^2$) in barrier properties at very modest flake concentrations. In addition, the fluid mechanics of the manufacturing (injection molding, blow molding) or application (coating) processes lead to orientation of the flakes that is largely parallel to the surface of the part and thus perpendicular to the direction of diffusion. In fire-retarding plastic parts manufactured by injection molding, the fountain flow and the shear gap-wise flow [9] result in highly oriented surface and subsurface regions, thus maximizing the barrier effect. The effect of flake concentration on the barrier properties have been studied, mainly in 2D [10–14] and models have been proposed, some of which [10,11], have been found to be in excellent agreement with computational results in two-dimensional RVEs [15–20]. However, all these results are strictly valid for ribbon composites and their relevance to three-dimensional reality is yet to be proven.

There have been some notable attempts to simulate transport across fully three-dimensional flake-filled composites. Nagy and Duxbury [21] carried out random walk computations in large-scale 2D and 3D geometries containing randomly placed unidirectional square-shaped platelets (sticks in 2D) of finite volume. They concluded that a quadratic polynomial of $(\alpha\phi)$, where (α) is the flake aspect ratio and (ϕ) the total flake volume fraction, can represent the BIF of such a composite over a wide range of concentrations, up to $\alpha\phi = 30$ in 3D configurations. The coefficients of this polynomial were determined by fitting computational results. Lusti et al. [22] presented a small number (40 geometries) of finite element simulation results in systems containing ~ 50 disks (aspect ratio 3, 10 and 100) dispersed randomly in a cubic RVE. They presented the first quantitative comparison between randomly oriented and aligned composites, expressing the difference in terms of a dimensionless parameter. Greco et al. [23,24], considered composites containing stacks of unidirectional disks; a total of 85 sim-

* Corresponding author.
E-mail address: athpapathan@mie.uth.gr (T.D. Papathanasiou).

https://doi.org/10.1016/j.ijheatmasstransfer.2020.119962
0017-9310/

ulations were run, in which orientation angle, the number of disks in a stack and the volume fraction varied. Greco [25], carried out 3D simulations also in disk-containing systems, in which the volume fraction, the aspect ratio (from 10 to 50) and the orientation angle were varied. Recently, Roding at al. [26] presented results of a large-scale study in systems each containing 1000 disks of circular or elliptical shape. They carried out ~ 1000 transient diffusion simulations, using a dynamic random walk particle tracking scheme. After [21] these were the first dynamic simulations for transport across flake filled systems and also the first attempt to model large-scale 3D systems. The influence of several morphological factors, such as flake misorientation, flake shape, flake thickness and flake polydispercity, was discussed. The works of [26] and [21] not-withstanding, it is fair to say that there has been no detailed study of three-dimensional diffusion in flake composites that covers a comprehensive range of the pertinent parameters. Beyond disks or squares, the effect of the flake shape on effective diffusivity remains largely unknown, even though hexagonal flakes are known to occur, (eg. in Graphene, MgO_2, hBN) - with the exception of the work of [27] who suggested a heuristic modification of the model of Cussler et al. [11] to be used in the case of hexagonal flakes. In addition, the effect of misorientation has only received spotty attention and remains to be quantified. Finally, the relevance of existing and well-studied models for fully-aligned systems [10–12] to three-dimensional reality is not proven. In fact, the study of Roding [26] has raised significant questions on the validity of existing 2D models. In this study we carry out a comprehensive (~ 3000 simulations) computational study of steady state diffusion in three-dimensional, multi-particle (up to 4000 flakes in each RVE) and periodic RVEs with the objective of giving answers to some of these questions.

2. Computational

Steady-state diffusion computations in three-dimensional Representative Volume Elements (RVEs) were carried out using the open source package OpenFoam. Each RVE is a parallepiped of dimensions *L, H, D* (along the *X, Y* and *Z* axes respectively) and contains a number (*N*) of flakes placed in random positions. We consider flakes of square, circular and hexagonal shape, as shown in Fig. 1. For the purpose of geometry generation, the circular flakes are inscribed in the corresponding rectangular flake and the hexagonal flake is inscribed in the corresponding circular geometry. The thickness dimension of the flakes was taken to be zero; this is not far from reality since in flake systems of practical importance flake thickness is very small compared to the planar dimensions. We define the planes that are formed from the *X-Y* axis, *X-Z* axis and *Y-Z* axis as *PXY, PXZ* and *PYZ* respectively (Fig. 2). The plane *PXZ* is perpendicular to the direction of diffusion (*Y*); *PXY* is perpendicular to the *Z*-axis where the flake rotation is taking place and *PYZ* is normal to the *X*-axis. The diffusion direction is taken to be along the *Y*-axis with $C = 0$ at $y = 0$ and $C = 1$ at $y = H$. The equation solved is the steady-state diffusion equation :

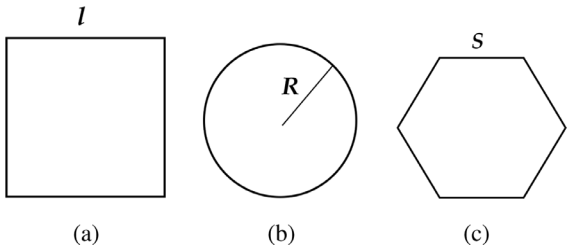

Fig. 1. Flake shapes considered in this study with their geometrical characteristics. *l* is the side of the square flake, *R* is the radius of the disk and *S* the side of the hexagon.

$$\nabla^2 C = 0 \tag{1}$$

The above equation was solved on RVEs generated using an in-house software solution that can create any variety of 2D and 3D RVEs with any combination of boundary and geometrical periodic conditions, including a user-specified number of flakes with any combination of sizes, shapes, spatial distributions and orientations. Subsequently the geometry files were imported to the mesh generator GMSH [28] and a triangular mesh was created with element count in the order of 100 M. Finally the simulations were solved using the OpenFoam toolkit [29].

The boundary conditions on the top and bottom surfaces of the unit cell are:

$$C_{(XY\,plane),Y=0} = 0 \quad \text{and} \quad C_{(ZX\,plane),Y=1} = 1 \tag{2}$$

Periodic conditions are applied at the sides of the RVE, namely

$$C_{(XY\,plane),X=0} = C_{(XY\,plane),X=1} \quad \text{and} \quad C_{(ZX\,plane),Y=0} = C_{(ZX\,plane),Y=1} \tag{3}$$

In 2D models, use of periodic conditions has been shown [15] to eliminate artifacts due to the shape of the unit cell and we see, from the results shown in Fig. 3, that this is true in 3D models as well.

The flakes are placed within the RVE using a random sequential addition procedure, in which random numbers assign the centroid coordinates of the flake. For a flake to be placed in the chosen position a triangle-triangle collision detection algorithm [30] was used since each flake is represented as a combination of triangles. If any triangle of the candidate flake overlaps with any triangle of the pre-existing flakes the position is rejected and a new combination of coordinates and appropriate angle is chosen until the RVE is filled with the desired number of flakes or a predetermined number of tries (10^7) is reached. During the collision detection stage a small safety distance between flakes was introduced in order to

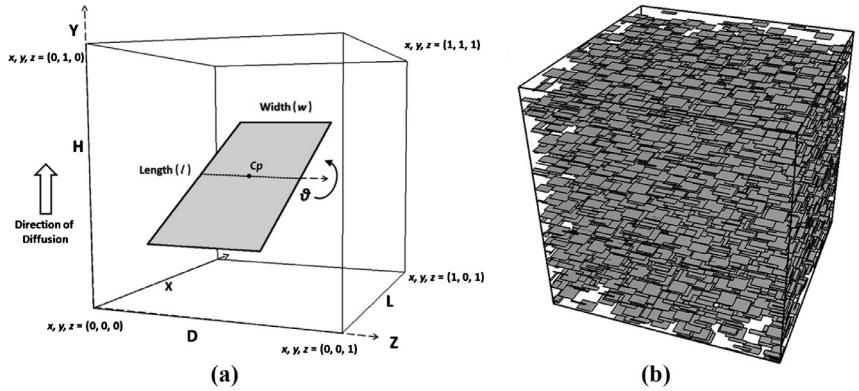

Fig. 2. (a) Schematic of the RVE and the geometrical characteristics of rectangular flakes. (b) a sample geometry containing $N = 4000$ square flakes at $\theta = 0^\circ$.

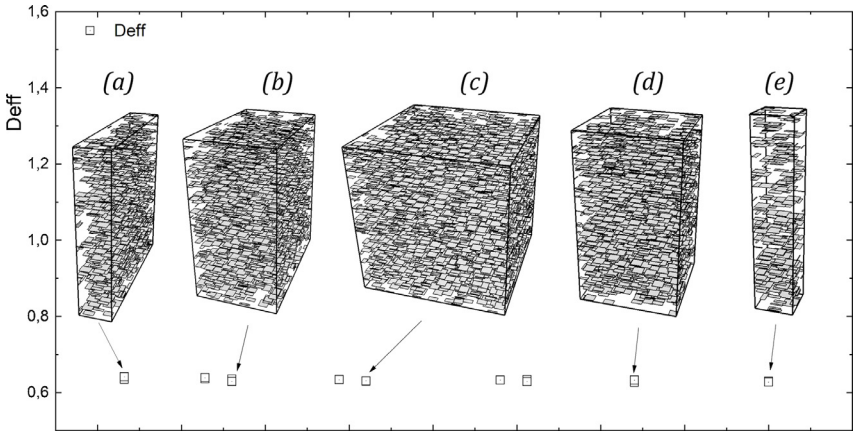

Fig. 3. Invariance of computational results for D_{eff} with size/shape of the RVE. Shown are values of D_{eff} calculated for various sizes and shapes of RVE's at $\theta = 0$ and having $M = 0.25$. In all cases the height of the RVE was kept constant. In (a) and (b) the height and depth were kept constant ($H = D = 1$) and the length was changed ($L < H$). In case (c) the RVE is a cube of unit length ($L = H = D = 1$). In (d) and (e) the depth and the length changed while L and D are kept equal ($L = D < H$). The middle case (c) has $N = 4000$ flakes. In the other cases the number of flakes (N) was changed accordingly in order to keep the flake number-density, $N/\Delta V$, and thus the scale M, constant.

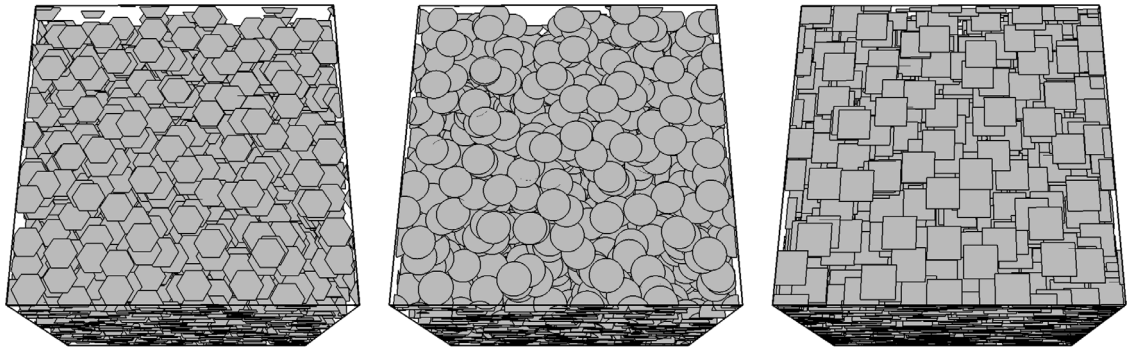

Fig. 4. Example geometries containing oriented flakes at $\theta = 0$ and various shapes. (a) hexagonal, (b) disk and (c) square. In all cases $N = 4000$.

avoid the creation of degenerate cells at the later stage of meshing. In randomly oriented configurations, the orientation vectors are assigned random values and the flakes are rotated at the X axis then the Y axis and finally at the Z axis. In the cases where the flakes are unidirectional, the rotation is applied only to the Z axis thus rotating the flakes perpendicular to the direction of diffusion, as illustrated in Fig. 2a. In Fig. 4 we can see additional example geometries of various shapes. The RSA algorithm used in this study ensures spatial homogeneity at the unit cell scale, while allowing for randomized small-scale aggregation, as was shown for 2D systems in Tsiantis and Papathanasiou [31]. Specifically in our work, the RVE was subdivided into a number of equal-sized voxels and it was verified that each voxel contained, on average (over the several realizations used at each level of $(\alpha\phi)$ and (θ)), the same number of flakes.

Solution of Eq. (1) supplies the concentration (C) and the concentration gradient ($\partial C/\partial n$) at each position of the domain. Fig. 5 shows a representative concentration field as well as a representative distribution of the corresponding flux field on the top surface of the RVE. Once the normal gradient ($\partial C/\partial n$) is computed on the top surface, an effective diffusivity (D_{eff}) of the unit cell can be calculated from Fick's law as:

$$D_{eff} = \frac{H \cdot D_0}{\Delta C \cdot D \cdot L} \int_0^D \int_0^L \frac{\partial C}{\partial n} dxdz \tag{4}$$

The so computed D_{eff} is the D_{yy} principal diffusivity that will be used in later section of this paper. In the following we will investigate the effect of flake size, shape, orientation and number density on the computed effective diffusivities. In the process we will propose a novel scaling that allows for a generalization of the observed behavior.

3. Results and discussion

3.1. Scaling of the results

At first we will focus our attention on the analysis and scaling of computational results. A suitable scale should be based on observations [26] that, among various parameters, the flake area and flake shape (elongated vs. square) affect the effective diffusivity. We have therefore chosen to represent our results in terms of a dimensionless parameter (M) defined as:

$$M = \frac{N \cdot (A)^2}{\Delta V \cdot (P)} \tag{5}$$

where (A) is the flake area, (P) its perimeter, ΔV is the volume of the RVE and the ratio (A/P) can be taken as a characteristic length of the flake, expressing also the flake shape. In the case of flakes of square shape, $A = l^2$ and $P = 4l$, resulting in

$$M^{sq} = \frac{N \cdot l^3}{4 \cdot \Delta V} \tag{6}$$

This result is consistent with earlier work in 2D flake systems [10,18], where it was shown that for flakes of zero thickness (in 2D these are represented by straight lines) a suitable scale is $N(l/H)^2$. The expressions for (M) in the case of disk-shaped and hexagonal

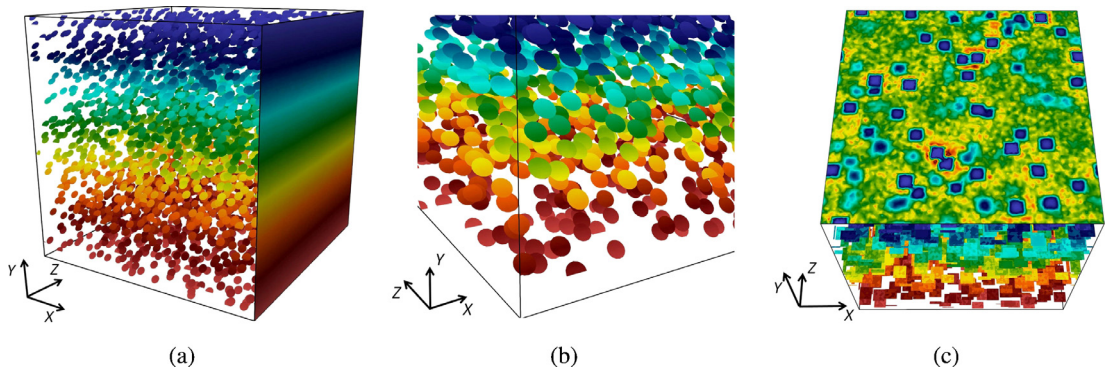

Fig. 5. Concentration fields in a 3D flake system containing randomly placed circular and rectangular flakes. (a) & (b) show circular flakes oriented at 45° to the direction of diffusion. (a) shows the concentration distribution, along a clipping plane at $Z = 1$, from the bottom of the RVE where $C = 1$ (colored red) to the top where $C = 0$ (colored blue) in the periodic surface of the RVE and on the flakes. On the middle (b) a close-up view is shown near the bottom of the RVE (the colors in the image are out of scale for illustration purposes). (c) Shows a typical flux distribution on the top surface of an RVE with square flakes. The placement of flakes near the top surface can be inferred from the local variations in the flux field. (For interpretation of the references to colour in this figure legend, the reader is referred to the web version of this article.)

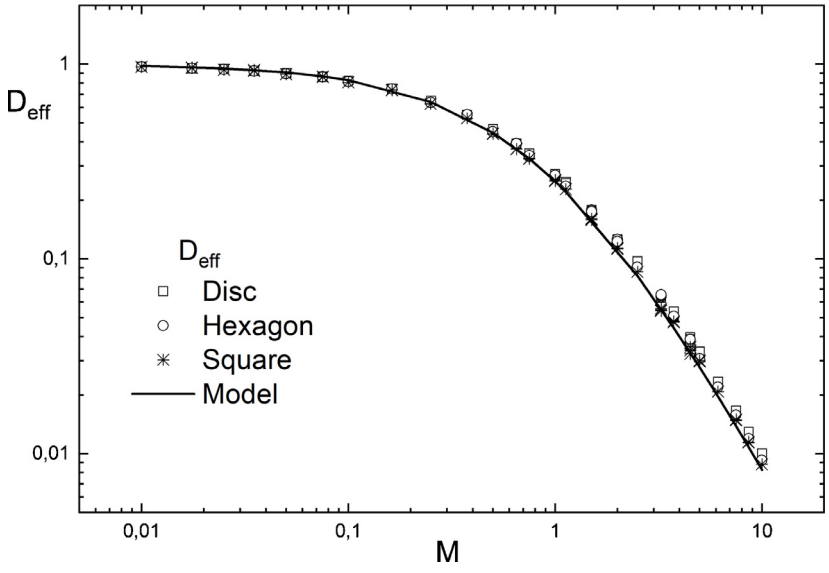

Fig. 6. Computational results obtained for different geometries and their comparison to Eq. (8). The formula used in the computation of (M) is different at each geometry, depending on flake shape (Eqs. (6) and (7) for flakes of square, disk and hexagon shape respectively).

flakes can be shown to be

$$M^c = \frac{1}{2}\frac{N}{\Delta V}\pi R^3 \quad \text{(circular)}, \quad M^h = \frac{27}{24}\frac{N}{\Delta V}S^3 \quad \text{(hexagonal)} \quad (7)$$

Our results for all flake shapes and concentrations, scaled in terms of the parameter (M), are summarized in Fig. 6. It is observed that use of the scale (M) collapses all data, irrespective of flake shape, on a single master curve. The form of the scaled data suggests that the effective diffusivity (D_{eff}) of a three-dimensional flake composite can be expressed as a power function of (M). The simplest possible such function which follows our results very closely, is

$$D_{eff} = D_0 \frac{1}{(1+M)^2} \quad (8)$$

in which the scale (M) is based on the general definition of Eq. (5) and is expressed by Eqs. (6) and (7) for the case of square, disk and hexagonal shaped flakes. The form of the power function of Eq. (8) is in line with earlier studies in 2D systems (10), (18) and it essentially confirms, also in 3D, that in systems with flakes aligned perpendicular to the direction of macroscopic transport, the *BIF* will asymptotically grow with the square of the appropriate scale, in our case (M).

We can easily notice from Eqs. (6) and (7) that M scales with a power of (3) of the corresponding flake characteristic length. This leads to inclusions whose size grows fast with (l), as can be seen in Fig. 7 where comparisons between geometries corresponding to various M for square geometries are shown. While at large values of (M) (Fig. 7) the flake dimensions seem large compared to the RVE, we have shown that the use of periodic geometries and periodic boundary conditions eliminates the edge effects even in extremely elongated RVEs (Fig. 3).

3.2. Relation to earlier work

As elaborated in the Introduction, all previous studies were concerned with disk-shaped or square flakes. These are geometries in which a definition of the flake aspect ratio (α) can be given without much ambiguity. It is natural therefore that the product $(\alpha\phi)$, (ϕ) being the flake volume fraction, was the scale of choice. For the case of 3D flakes of square shape $(\phi = Nl^2t/\Delta V)$, the *BIF* was found in Nagy and Duxbury [21] to be represented by

$$BIF = 1 + C_1(\alpha\phi) + C_2(\alpha\phi)^2 \quad (9)$$

In Eq. (9), t is the flake thickness and $\alpha = l/t$ is a definition of the flake aspect ratio. The constants C_1 and C_2 were determined in Nagy and Duxbury [21] by fitting computational results of $(BIF - 1)/(\alpha\phi)$ vs. $(\alpha\phi)$ and were found to be $C_1 = 0.44 \pm 0.03$

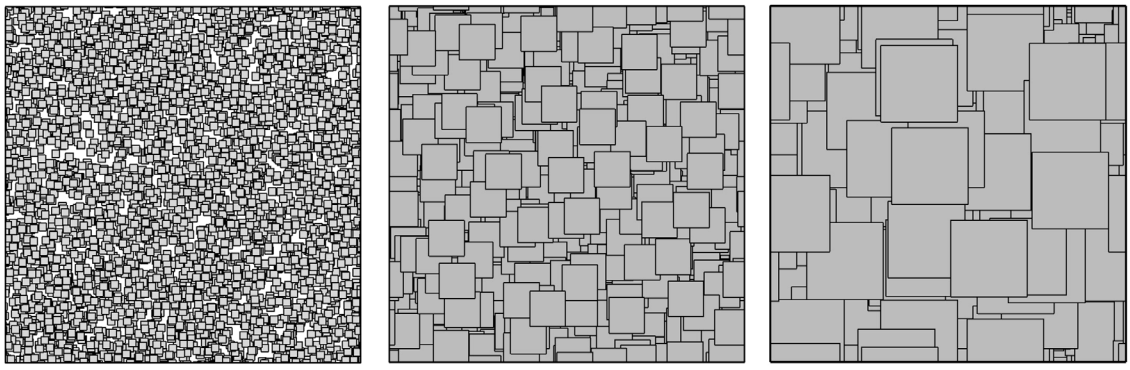

Fig. 7. Scaling of geometries according to different M. The top view of the RVE is shown with square geometries at $\theta = 0$. $M = 0.01$ (left), $M = 1.0$ (center) and $M = 10$ (right). In all cases the dimensions of the unit cell remain the same therefore the relative size of the flakes is clearly seen.

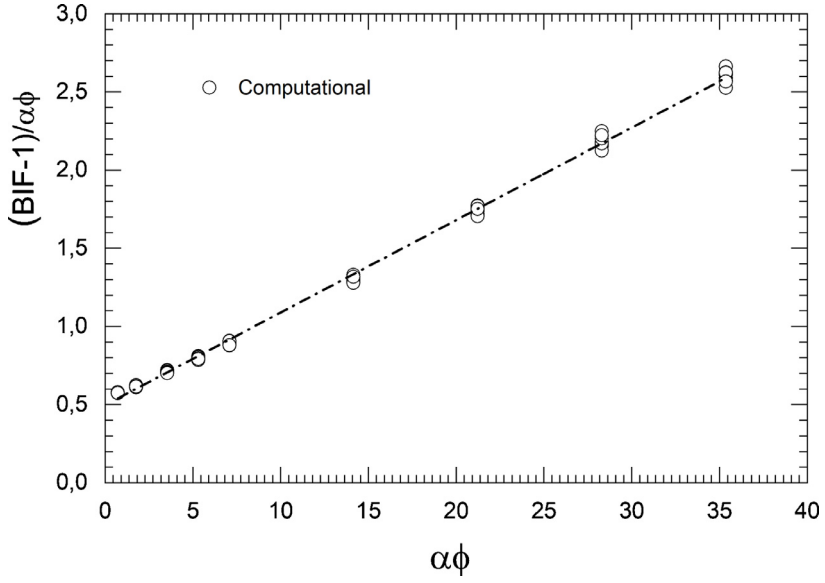

Fig. 8. Computational results for square flakes at $\theta = 0$ plotted as suggested by Eq. (9). The intercept gives $C_1 = 0.4987$ and this compares favourably with the value of 0.5 anticipated from Eq. (11). The slope gives $C_2 = 0.0591$; this is very close to the result $C_2 = 0.05$ of [21] and also compares to $0.0625 = 1/16$ anticipated from Eq. (11).

and $C_2 = 0.05 \pm 0.005$. It is instructive to compare the results of the proposed model (Eq. (8)) to those of [21], and Eq. (9). According to Eq. (8), $BIF = (1+M)^2 = 1 + 2M + M^2$. For the case of square flakes Eq. (6) can be rearranged by dividing and multiplying with flake thickness (t) so that

$$M^{sq} = \frac{1}{4} \cdot \frac{N \cdot l^2 t}{\Delta V} \cdot \frac{l}{t} = \frac{\alpha\phi}{4} \tag{10}$$

Therefore, for the case of square flakes, our proposed model for the BIF gives

$$BIF_{sq} = (1 + M_{sq})^2 = 1 + \frac{1}{2}\alpha\phi + \frac{1}{16}(\alpha\phi)^2 \tag{11}$$

resulting in $C_1 = 0.5$ and $C_2 = 0.0625$. A comparison between our results and Eq. (9) is shown in Fig. 8 in which we plot $(BIF - 1)/\alpha\phi$ vs $\alpha\phi$.

The values for C_1 and C_2 obtained from our computational results are very close to those of [21], the differences probably originating from the different numerical method used and also from the fact that in our study the flake thickness has been neglected, flakes being in our case essentially 2D entities. In the case of circular and hexagonal flakes, it can be shown that the concentration metric ($\alpha\phi$) is related to the scaling parameters M^h and M^c as $\alpha\phi = 4M^c$ for the case of circular and $\alpha\phi = M^h$ for the case of hexagonal flakes. In obtaining these, the aspect ratio of the disk is defined as $\alpha = 2R/t$, while for the hexagon, $\alpha = L_C/t$, where L_C is a characteristic length defined as $(Area)/(Perimeter)$ ($L_C = \sqrt{3} \cdot S/4$). It is therefore,

$$BIF^c = 1 + \frac{1}{2} \cdot \alpha\phi + \frac{1}{16} \cdot (\alpha\phi)^2 \tag{12}$$

yielding $C_1 = 1/2$ and $C_2 = 1/16$ for disks and

$$BIF^h = 1 + 2\alpha\phi + (\alpha\phi)^2 \tag{13}$$

yielding $C_1 = 2$ and $C_2 = 1$ for hexagons. If, alternatively, the aspect ratio of the hexagon is based on its longest diagonal, which is $2S$, then it can be shown that

$$\alpha\phi = \frac{8}{\sqrt{3}} M^h \tag{14}$$

In that case,

$$BIF^h = 1 + \frac{\sqrt{3}}{4}\alpha\phi + \frac{3}{64}(\alpha\phi)^2 \tag{15}$$

yielding $C_1 = \sqrt{3}/4$ and $C_2 = 3/64$.

The computational results for disk-shaped and hexagonal flakes are plotted as suggested by Eqs. (12), (13) and (15) in Fig. 9. As in the case of square flakes, we find that the computational results

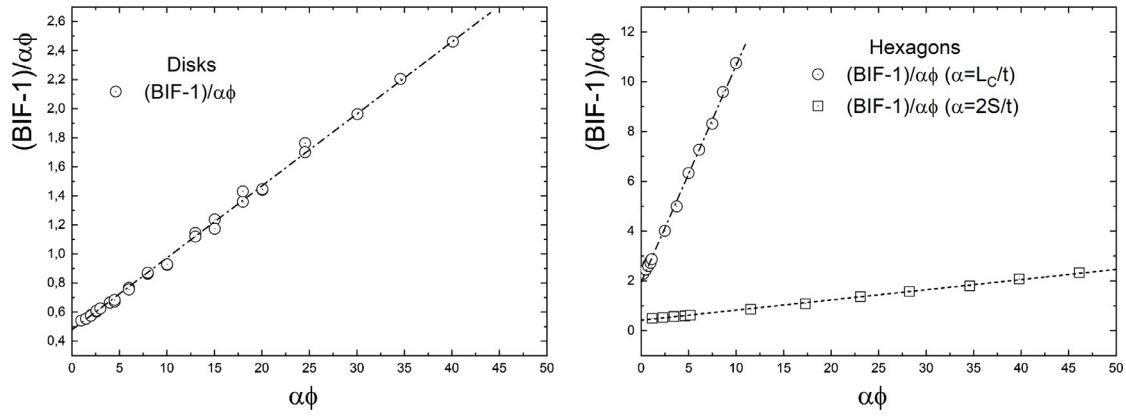

Fig. 9. Computational results for circular and hexagonal flakes at $\theta = 0$ plotted as suggested by Eq. (9). The intercept gives $C_1 = 0.4715$ for disks and $C_1 = 1.91$ for hexagons when the aspect ratio is based on L_C. These compare with the values of 1/2 and 2 suggested by Eqs. (12) and (13). The slopes give $C_2 = 0.0498$ and $C_2 = 0.876$ and these compare to 1/16 (for disks) and 1.0 (for hexagons) suggested by Eqs. (12) and (13). In Fig. 9b the linear fit corresponding to the alternative definition of the aspect ratio (based on the long diagonal of the hexagon, Eq. (15)) is also shown. The corresponding best-fit values are $C_1 = 0.4015$ and $C_2 = 0.0413$.

Table 1
Values of the polynomial coefficients C_1 and C_2 obtained from our computational results (Figs. 8 and 9) for various flake shapes.

	Squares	Squares [21]	Disks	Hexagons	
				$(\alpha = L_C/t)$	$(\alpha = 2S/t)$
C_1	0.4987	0.44	0.4715	1.910	0.4015
C_2	0.0591	0.05	0.0498	0.876	0.0413
Implied from Eq. (8)					
C_1	0.5000		0.5000	2.0	0.43250
C_2	0.0625		0.0625	1.0	0.04687

follow closely the behavior suggested by Eq. (9), with suitably defined coefficients. Our results are summarized in Table 1.

3.3. Comparison to predictions of existing models

In the following we compare the results of our 3D computations and the proposed model (Eq. (8)) with the predictions of frequently used models for the *BIF* of flake composites, namely those of [10,11]. The relevant equations are:

$$\frac{D_o}{D_{eff}} = \frac{(1+\alpha\phi/\lambda)^2}{1-\phi} \tag{16}$$

and

$$\frac{D_o}{D_{eff}} = 1 + \frac{\alpha^2\phi^2}{\beta(1-\phi)} \tag{17}$$

where (λ) and (β) are geometrical factors, reflecting the tortuous path the diffusing species follows as it travels around individual flakes. It is understood that these geometrical factors will depend on flake shape. In the original work of [11] it was suggested that $\lambda = 3$. Computational results of [17] in 2D geometries (in which flake cross sections are represented as lines or rectangles) have given a best fit for $\lambda = 2.5$. In the present study the flakes are infinitely thin and thus $1-\phi \sim 1$, yielding

$$BIF = (1+\alpha\phi/\lambda)^2 = 1 + \frac{2}{\lambda}\alpha\phi + \frac{1}{\lambda^2}(\alpha\phi)^2 \tag{18}$$

Comparing this expression to the previously derived expressions for the *BIF* of composites containing square, circular and hexagonal flakes, we are able to obtain estimates of the geometrical parameter (λ) for each flake shape.

1. For squares $\lambda = 4$, $(2/\lambda = 0.5$ and $1/\lambda^2 = 1/16)$
2. For disks $\lambda = 4$, $(2/\lambda = 1/2$ and $1/\lambda^2 = 1/16)$, when aspect ratio is defined as $\alpha = 2R/t$.
3. For hexagonal
   (a) $\lambda = 1$, $(2/\lambda = 2$ and $1/\lambda^2 = 1)$, if aspect ratio is based on characteristic length, $L_C = \sqrt{3}\cdot S/4$
   (b) $\lambda = 8\sqrt{3}/3$, $(2/\lambda = \sqrt{3}/4$ and $1/\lambda^2 = 3/64)$ if the longest flake diagonal is used in the calculation of the aspect ratio of the flake $(\alpha = 2S/t)$. In regards to Eq.(17), comparison with our results gives $\beta = 16$ for squares and disks and $\beta = 1$ for hexagonal flakes $(L_C = \sqrt{3}.S/4)$.

For the particular case of hexagonal flakes, [27] have proposed an expression for the *BIF*, based on a generic model of the form of Eq. (17) and using heuristic diffusion path arguments. The expression offered is

$$BIF = 1 + \frac{2}{27}(\alpha\phi)^2 \tag{19}$$

While omission of the linear term is bound to affect the predictions of this model, especially in the dilute and semi-dilute regimes, the coefficient of the quadratic term will determine the asymptotic growth of *BIF* vs. $(\alpha\phi)$ in the concentrated regime. This coefficient, $2/27 = 0.074$, compares with the coefficient 0.0413 (Table 1) obtained from our computational data for hexagonal flakes (Fig. 9b) when the aspect ratio is based on the flake longest diagonal and to the value $3/64 = 0.0469$ inferred from Eq. (15). Note that this value would be very different if the flake aspect ratio were to be determined by using a different characteristic length.

In regards to micromechanics-based models, our result, expressed by Eq. (8), is found to be in good agreement with the work of [32]. That model has as its starting point the solution of Fricke [33] for the thermal conductivity of composites reinforced with spheroidal inclusions. In the limit of non-conductive, high-aspect-ratio oblate spheroids, the model of [32] for the effective diffusivity of the composite takes the form

$$\frac{D_{eff}}{D_0} = (1-\phi)^K \tag{20}$$

where (K) is a function of the spheroid aspect ratio (α), namely $K = (3L+2)/3L(2-L)$. According to [32] the value of (L) is 2/3 at $\alpha = 1$ (spherical particle) and decays $\sim 1/\alpha$ for high aspect ratios. A formula that reconciles these requirements is $L = (2/3\alpha)$. This yields $K \sim \alpha/2$ for high aspect ratio, impermeable oblate spheroids; in deriving this we used $\alpha + 1 \sim \alpha$ and $3\alpha - 1 \sim 3\alpha$, since $\alpha \gg 1$. The binomial theorem can be used to expand Eq. (20) yielding for

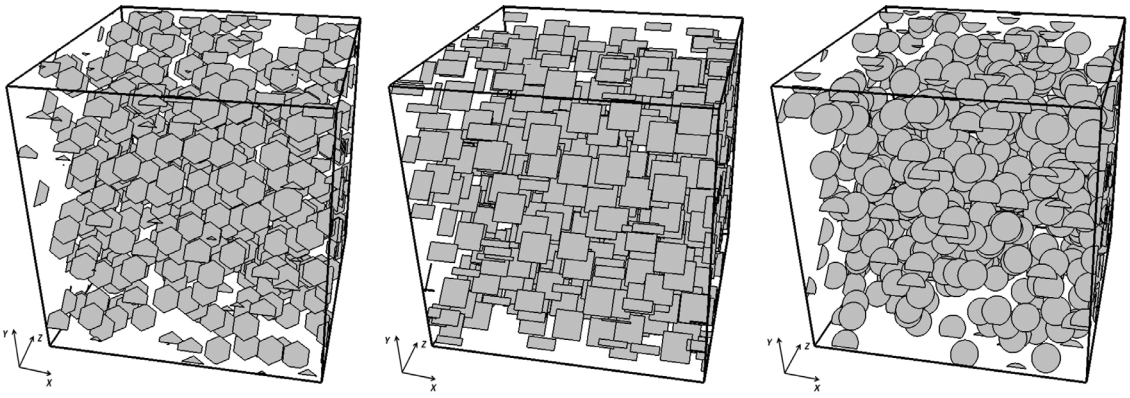

Fig. 10. 3D oriented flake configurations at $\theta = 45^{\circ}$. Number of flakes has been reduced to 500 for visual clarity. All flakes are rotated around the *X*-axis.

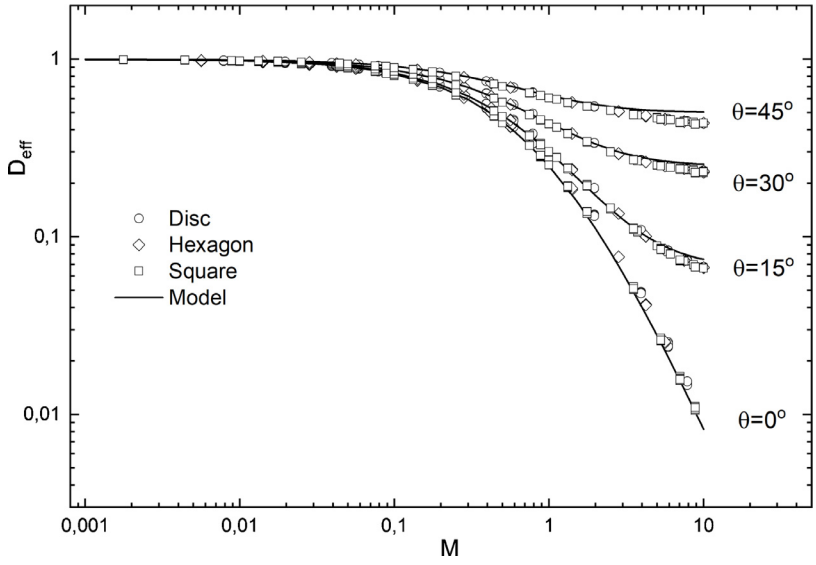

Fig. 11. Computational results (points) and model predictions (lines) for various flake shapes and orientations. Model predictions based on Eq. (23).

the *BIF*, (keeping terms up to 2nd order in $(\alpha\phi)$ and ignoring terms ~ $(1/\alpha)^n$ in the expansion coefficients).

$$BIF = (1-\phi)^{-K} = 1 + \frac{1}{2}\alpha\phi + \frac{1}{8}(\alpha\phi)^2 + HOTs \tag{21}$$

The Higher Order Terms in Eq. (21), up to 5th order, are $(\alpha\phi)^3/48$, $(\alpha\phi)^4/384$ and $(\alpha\phi)^5/3840$ - again, neglecting terms of $O(1/\alpha)^n$ in determining the expansion coefficients. This result is similar to Eqs. (11) and (12) of our work, yielding similar predictions up to the semi-dilute regime ($\alpha\phi \sim 2$) and overestimating the BIF afterwards. In fact they are identical in the linear term, which is expected since the result of [32] has as starting point the solution to the corresponding diffusion problem in the dilute regime.

3.4. The effect of flake orientation

Having proposed Eq. (8), we further investigate the effect of flake misalignment, by considering unidirectional systems in which the flakes form an angle (θ) with the direction of diffusion, as shown in Fig. 10. We carry out simulations for $\theta = 15^{\circ}$, 30° and 45°, for various flake shapes and dimensions. In all simulations $N = 4000$. If D_{11} and D_{22} are the principal values of the two-dimensional diffusivity tensor, $\boldsymbol{D}$, the diffusivity tensor $\boldsymbol{D'}(\theta)$ corresponding to flakes oriented at an angle θ as shown in Fig. 10, can be determined through the tensor transformation relation $\boldsymbol{D'} = \boldsymbol{QDQ^T}$, where $\boldsymbol{Q}$ is the rotation tensor. Hence,

$$\frac{D_{eff}(\theta)}{D_0} = D_{11}\cos^2(\theta) + D_{22}\sin^2(\theta) \tag{22}$$

For D_{11} we use the model derived in this study, expressed by Eq. (8), while D_{22} can be described by the model of Nielsen [34], in line with similar work in 2D [17]. Since the flake thickness is insignificant in our work, flakes being essentially two-dimensional, $\phi \sim 0$ and $D_{22} = D_0$. Therefore, a model for $D_{eff}(\theta)$ is:

$$\frac{D_{eff}(\theta)}{D_0} = \frac{1}{(1+M)^2}\cos^2\theta + \sin^2\theta \tag{23}$$

Fig. 11 summarizes the results of our computations as well as the predictions of Eq. (23). It is clear that misalignment reduces the barrier factor. In a manner similar to what has been observed in 2D systems, our results also show that when $\theta > 0$ the *BIF* does no longer grow with the square of (M), but that it approaches a plateau value as (M) increases. From Eq. (23) it is clear that this plateau value is a function of the misalignment angle (θ).

4. Conclusions

We have investigated computationally three dimensional transport in composite systems consisting of randomly placed unidirectional flakes of square, circular and hexagonal shape. Analysis of

the results reveals that use of a scale of the form $M = (N/\Delta V) \cdot (A) \cdot (A/P)$ is capable of reducing the *BIF* for composites containing flakes oriented perpendicular to the direction of macroscopic diffusion on one single master curve. This master curve is represented by a power function of the form $BIF = (1 + M)^2$. The proposed scale requires knowledge of the number density and dimensions (area, perimeter) of the flakes. We show how the common description of the *BIF* as a quadratic polynomial of $(\alpha\phi)$ can be deduced from our general model and we find the appropriate polynomial coefficients for each flake shape. We show that beyond disks and squares, these coefficients are very sensitive to the length used in the calculation of the flake aspect ratio (α). Our model is also compared to established models which, being developed using heuristic diffusion path arguments, include an adjustable geometric constant; we derive values for these geometrical constants at each flake shape. Additional simulations in systems in which the flakes form an angle (θ) with the direction of the macroscopic diffusion, have resulted in a model for the *BIF* in terms of the principal diffusivity and (θ); this is found to be in very good agreement with computational results, which show that while the *BIF* increases with increasing (M), this increase is no longer monotonic but, instead, *BIF* approaches an asymptotic plateau value which is determined by (θ). It should be pointed that due to the similarity in the governing equation, the formulation and methods implemented in this study, as well as the results derived, could be directly applicable to analyzing heat transfer in flake-filled composites. In that case, the predicted reduction in effective diffusivity expressed through Eq. (8) should be usable to predict an upper limit in the reduction in effective thermal conductivity of such composites reinforced with insulating flakes. A notable difference between the diffusion problem dealt with in the present study and the corresponding heat transfer problem lies in the conductivity of the dispersed phase (flakes). While it is perfectly within physical reality that flakes act as impermeable barriers to diffusing species, such an assumption is not so readily realized in heat transfer applications, in which conduction across flake thickness may be significant or even faster than conduction in the matrix material. In the case of high aspect ratio flakes, such as those considered in the present study, this would necessitate the adoption of special boundary conditions on the flake surface; we are working towards implementing such a capability within the OpenFoam computing environment.

Declaration of Competing Interest

The authors declare that they have no known competing financial interests or personal relationships that could have appeared to influence the work reported in this paper.

References

[1] A. Ophir, A. Dotan, I. Belinsky, S. Kenig, Barrier and mechanical properties of nanocomposites based on polymer blends and organoclays, J. Appl. Polym. Sci. 116 (1) (2010) 72–83, doi:10.1002/app.31285.

[2] S. Pavlidou, C.D. Papaspyrides, A review on polymer-layered silicate nanocomposites, Prog. Polym. Sci. 33 (12) (2008) 1119–1198, doi:10.1016/j.progpolymsci.2008.07.008.

[3] B. Tan, N.L. Thomas, A review of the water barrier properties of polymer/clay and polymer/graphene nanocomposites, J. Memb. Sci. 514 (2016) 595–612, doi:10.1016/j.memsci.2016.05.026.

[4] K. Bhunia, S. Dhawan, S. Sablani, Modeling the oxygen diffusion of nanocomposite-based food packaging films, J. Food Sci. 77 (2012) N29–38, doi:10.1111/j.1750-3841.2012.02768.x.

[5] J.M. Lagaron, E. Nunez, Nanocomposites of moisture-sensitive polymers and biopolymers with enhanced performance for flexible packaging applications, J. Plast. Film Sheeting 28 (2011) 79–89, doi:10.1177/8756087911427756.

[6] L. Xia, H. Wu, S. Guo, X. Sun, W. Liang, Enhanced sound insulation and mechanical properties of LDPE/mica composites through multilayered distribution and orientation of the mica, Compos. Part A 81 (2016) 225–233, doi:10.1016/j.compositesa.2015.11.023.

[7] B. Pajarito, M. Kubouchi, Flake-filled polymers for corrosion protection, J. Chem. Eng. Jpn. 46 (2013) 18–26, doi:10.1252/jcej.12we133.

[8] A. Dasari, Z.-Z. Yu, G.-P. Cai, Y.-W. Mai, Recent developments in the fire retardancy of polymeric materials, Prog. Polym. Sci. 38 (9) (2013) 1357–1387, doi:10.1016/j.progpolymsci.2013.06.006.

[9] T.D. Papathanasiou, 4-flow-induced alignment in injection molding of fiber-reinforced polymer composites, in: T.D. Papathanasiou, D.C. Guell (Eds.), Flow-Induced Alignment in Composite Materials, Woodhead Publishing Series in Composites Science and Engineering, Woodhead Publishing, 1997, pp. 112–165, doi:10.1201/9781439822739.ch4.

[10] N.K. Lape, E.E. Nuxoll, E.L. Cussler, Polydisperse flakes in barrier films, J. Memb. Sci. 236 (1) (2004) 29–37, doi:10.1016/j.memsci.2003.12.026.

[11] E.L. Cussler, S.E. Hughes, W.J. Ward, R. Aris, Barrier membranes, J. Memb. Sci. 38 (2) (1988) 161–174, doi:10.1016/S0376-7388(00)80877-7.

[12] M. Minelli, M.G. Baschetti, F. Doghieri, A comprehensive model for mass transport properties in nanocomposites, J. Memb. Sci. 381 (1) (2011) 10–20, doi:10.1016/j.memsci.2011.06.036.

[13] M. Minelli, M. Giacinti Baschetti, F. Doghieri, Analysis of modeling results for barrier properties in ordered nanocomposite systems, J. Memb. Sci. 327 (2009) 208–215, doi:10.1016/j.memsci.2008.11.021.

[14] M. Dondero, J.P. Tomba, A.P. Cisilino, The effect of flake orientational order on the permeability of barrier membranes: numerical simulations and predictive models, J. Memb. Sci. 514 (2016) 95–104, doi:10.1016/j.memsci.2016.04.064.

[15] A. Tsiantis, T.D. Papathanasiou, An evaluation of models and computational approaches for the barrier properties of coatings containing flakes of high aspect ratio, J. Coat. Technol. Res. 16 (2) (2019) 521–530, doi:10.1007/s11998-018-0130-z.

[16] X. Chen, T.D. Papathanasiou, Barrier properties of flake-filled membranes: review and numerical evaluation, J. Plast. Film Sheeting 23 (4) (2007) 319–346, doi:10.1177/8756087907088437.

[17] A. Tsiantis, T. Papathanasiou, The barrier properties of flake-filled composites with precise control of flake orientation, Mater. Sci. Appl. 08 (2017) 234–246, doi:10.4236/msa.2017.83016.

[18] A. Tsiantis, T.D. Papathanasiou, A closed-form solution for the barrier properties of randomly oriented high aspect ratio flake composites, J. Compos. Mater. 53 (16) (2019) 2239–2247, doi:10.1177/0021998318825295.

[19] T.D. Papathanasiou, A. Tsiantis, Orientational randomness and its influence on the barrier properties of flake-filled composite films, J. Plast. Film Sheeting 33 (4) (2017) 438–456, doi:10.1177/8756087916682793.

[20] M. Dondero, A.P. Cisilino, J.P. Tomba, Experimental validation of computational models for mass transport through micro heterogeneous membranes, J. Memb. Sci. 437 (2013) 25–32, doi:10.1016/j.memsci.2013.02.039.

[21] T.F. Nagy, P.M. Duxbury, Permeability and conductivity of platelet-reinforced membranes and composites, Phys. Rev. E 66 (2) (2002), doi:10.1103/physreve.66.020802.

[22] H. Lusti, A. Gusev, O. Guseva, The influence of platelet disorientation on the barrier properties of composites: a numerical study, Model. Simul. Mater. Sci. Eng. 12 (2004) 1201, doi:10.1088/0965-0393/12/6/013.

[23] A. Greco, A. Maffezzoli, Two-dimensional and three-dimensional simulation of diffusion in nanocomposite with arbitrarily oriented lamellae, J. Memb. Sci. 442 (2013) 238–244, doi:10.1016/j.memsci.2013.04.038.

[24] A. Greco, C.E. Corcione, A. Maffezzoli, Diffusion in oriented lamellar nanocomposite: numerical analysis of the effects of dispersion and intercalation, Comput. Mater. Sci 133 (2017) 45–51, doi:10.1016/j.commatsci.2017.03.011.

[25] A. Greco, Simulation and modeling of diffusion in oriented lamellar nanocomposites, Comput. Mater. Sci 83 (2014) 164–170, doi:10.1016/j.commatsci.2013.11.019.

[26] M. Röding, K. Gaska, R. Kádár, N. Lorén, Computational screening of diffusive transport in nanoplatelet-filled composites: use of graphene to enhance polymer barrier properties, ACS Appl. Nano Mater. 1 (1) (2018) 160–167, doi:10.1021/acsanm.7b00067.

[27] G.D. Moggridge, N.K. Lape, C. Yang, E.L. Cussler, Barrier films using flakes and reactive additives, Prog. Org. Coat. 46 (4) (2003) 231–240, doi:10.1016/S0300-9440(02)00180-7.

[28] C. Geuzaine, J.-F. Remacle, Gmsh: a 3-D finite element mesh generator with built-in pre- and post-processing facilities, Int. J. Numer. Methods Eng. 79 (2009) 1309–1331, doi:10.1002/nme.2579.

[29] H.G. Weller, G. Tabor, H. Jasak, C. Fureby, A tensorial approach to computational continuum mechanics using object orientated techniques, Comput. Phys. 12 (1998) 620–631, doi:10.1063/1.168744.

[30] T. Oller, A fast triangle-triangle intersection test, J. Graph. Tools 2 (2004), doi:10.1080/10867651.1997.10487472.

[31] A. Tsiantis, T.D. Papathanasiou, A novel FastRSA algorithm: statistical properties and evolution of microstructure, Phys. A 534 (2019) 122083.

[32] A.D. Drozdov, J.D. Christiansen, Micromechanical modeling of barrier properties of polymer nanocomposites, Compos. Sci. Technol. 189 (2020) 108002.

[33] H. Fricke, A mathematical treatment of the electric conductivity and capacity of disperse systems I. The electric conductivity of a suspension of homogeneous spheroids, Phys. Rev. 24 (5) (1924) 575–587.

[34] L.E. Nielsen, Models for the permeability of filled polymer systems, J. Macromol. Sci. 1 (5) (1967) 929–942, doi:10.1080/10601326708053745.